Annealing effect on physical characterisation and sensing properties of nanostructered AgO thin films

H. S. Ali [a], M. S. Sada [b,*], Y. I. Al-Rikabi [c], K. N. Hussein [d], N. F. Habubi [e], S. S. Chiad [f], M. Jadan [g,h]

[a] *Department of Physics, College of Education for Pure Sciences, University of Tikrit, Iraq*
[b] *Minsitry of Education, General Diroctorain the Province of Maysan, Iraq.*
[c] *Department of Science, College of Basic Education, University of Diyala, Iraq.* [d] *Department of Radiology, Al-Manara College for Medical Science, Iraq.*
[e] *Department of Radiation and Sonar Technologies, Al-Nukhba University College, Iraq*
[f] *Department of Physics, College of Education, Mustansiriyah University, Iraq.*
[g] *Department of Physics, College of Science, Imam Abdulrahman Bin Faisal University, P.O. Box 1982, 31441 Dammam, Saudi Arabia*
[h] *Basic and Applied Scientific Research Center, Imam Abdulrahman Bin Faisal University, P.O. Box 1982, 31441 Dammam, Saudi Arabia*

Thermal evaporation (TE)was employed to create thin coatings of AgO on glass substrates. The post-annealing temperatures for the deposited films were (100, 150, and 200), respectively. The XRD data demonstrate that when annealing temperature climbed from 100°C to 200°C, the intensity of (100) plane strengthened. Regardless of the temperatures used for post-annealing, the XRD spectra show that the films are polycrystalline and have a cubic structure. The average grain size was 15.39 nm, 16.30 nm, and 17.68 nm for the intended films. When the annealed temperature rises, the dislocation density and strain value decrease. The root mean square (RMS) roughness measured via AFM images decreased from 7.33 nm to 3.64 nm. Due to annealing at 200°C, the average particle size behaved similarly and reduced from 76.9 nm to 46.5 nm. The surface roughness exhibited the same behavior and dropped from 8.77 nm to 4.46 nm at 200 ºC. The sample annealed at 200°C had the highest absorbance values, whereas the sample annealed at 100°C had the highest transmittance values. As the film annealing increased, the absorption coefficient rose somewhat. The bandgap of AgO thin films falls from 1.59 eV to 1.44 eV with the rise of annealing. In contrast, the transmittance, refractive index, and Extinction coefficient also lower as the temperature rises. Sensitivity measurements indicated a reduction in sensitivity as the annealing temperature and gas concentration increased.

1. Introduction

Many research teams have been interested in silver oxide thin films recently [1–9], mainly because they have important uses as storage devices. Photovoltaic materials like AgO are used as active cathode in batteries, antimicrobial coatings, photocatalysts, and optical memory. There are several phases in the binary Ag-O system, containing Ag_2O, Ag_3O_4, AgO, Ag_4O_3, and Ag_2O_3 [4,5]. The most stable of these various molecules is Ag_2O. [6,7]. AgO thin film has a band gap of 1.2 to 3.4 eV [8,9]. Ag_xO is a thermodynamically unstable substance. At 220 °C, it breaks down into Ag_2O; at about 410 °C, it turns into metallic Ag and O_2 [10]. There are several ways to make silver

---

oxide thin films like; Reactive sputtering [4, 11–14] and electron-beam evaporation [15–16] are the main methods employed for depositing Ag_xO films. PLD is another approach [15, 17]. Electrochemical processes and chemistry [18, 19], electrochemical processes [20, 21], and thermal evaporation [22–23]. We chose this method because the final one offers advantages, including improved substrate temperature, controllable excitation energy on oxygen pressure, and cost-effectiveness. Using the thermal evaporation process, we created undoped thin films from AgO. It investigated how annealing affected the structural, morphological, and specific optical characteristics of AgO films.

2. Experimental

Thermal evaporation was used to deposit Ag films from a high-purity Ag (99.99%) target onto glass substrates. Once the required vacuum of 10^{-5} Torr has been reached, a strong current of 225 A is gently conducted through the boat, causing silver to evaporate and deposit itself as thin coatings of Ag on surfaces. Deposition takes place for 15 minutes, and 25 cm separate the source and the substrate. To create silver oxide films, the obtained films were annealed in a thermal oven for 2 hrs. at 100°C (sample 1), 150°C (sample 2), and 200°C (sample 3). Film thickness was reported to be 120 nm ±10 nm using the weighing balance, AFM was used to analyze the samples' surface morphology while in ambient conditions and functioning in the tapping mode. The morphology was employed using SEM. A UV-Vis spectrophotometer and an integrating sphere were used to measure the transmittance and reflectance. Gas sensing measurements were conducted using the testing system depicted in Figure (1).
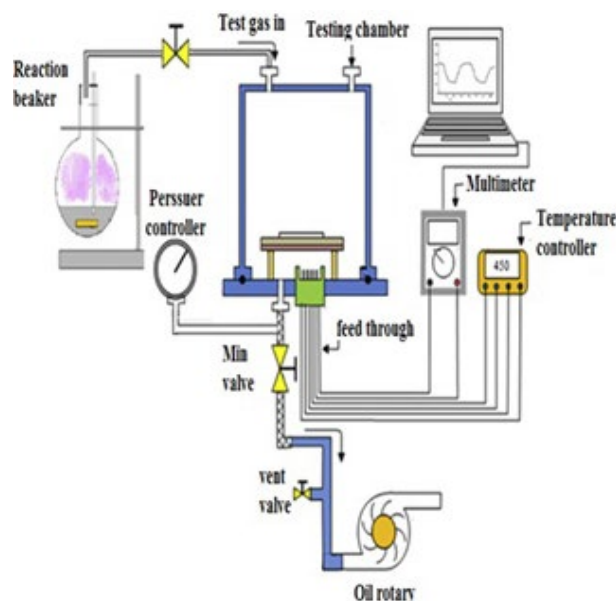

Fig. 1. Schematic diagram of gas sensor system.

3. Results and discussions

XRD patterns for AgO thin films on a glass substrate are shown in Figure (2). As seen in Fig. (2), AgO XRD patterns Films are polycrystalline materials, as may be offered. Figure 1's revelations include There are several peaks at the diffraction angles of 34.18°, 37.13°, 52.58°, and 62.31° that are, respectively, attributable to the (002), (111), (020), and (220) planes¨[20], and planes which have been compared with the standard XRD diffraction date standard JCPDS card No, demonstrate the preferred growth along (100) orientation, with the peak produced for thin film

at 2 = 34.18° having a considerably greater intensity (43-1038) Where it was discovered, tetrahedral-shaped thin films are made [24].

Through Debye-Scherrer's relation, it was calculated the crystallite size (*D*)[26-28]

$$D = \frac{0.9\lambda}{\beta cos\theta}$$ (1)

where β is FWHM and λ is X-ray wavelength. The results are shown in Table 1, demonstrating that *D* increases for higher annealing temperatures of 200°C compared to annealing at 100°C. It is discovered that *D* ranges from 15.39 nm to 17.68 nm in response to a systematically rising annealing temperature (T_{an}) of 200°C [29].

We may calculate the dislocation density using the relationships in equation 2. [30-32]

$$\delta = \frac{1}{D^2}$$ (2)

The dislocation density is 42.18, 37.62, and 31.99 with various annealing temperatures [31, 32].

We can use the relations in equation 3 to evaluate the lattice strain (*ε*) [33-35]:

$$\varepsilon = \frac{\beta cos\theta}{4}$$ (3)

The strain is discovered to be 22.51, 21.26, and 19.60 [34]. Table 1 provides the computed structural parameters. 1

Figure (3) illustrates the relationship between the prepared films' FWHM, grain size, dislocation density, and strain. It mentions the inverse link between *D* and other factors. Figure (2) shows strain vs annealing temperature for Structural parameters $S_{par.}$.
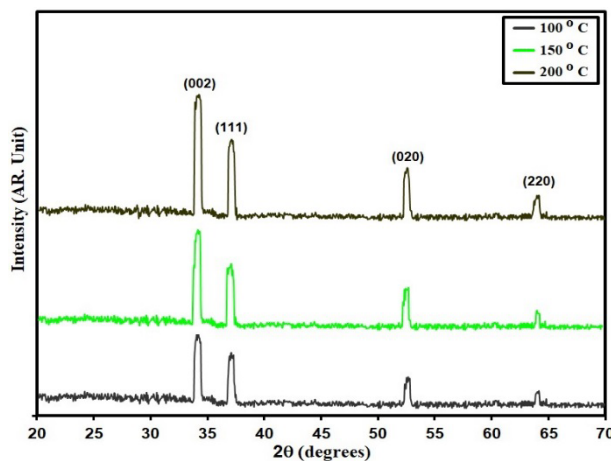

Fig. 2. XRD of deposit films.

Table 1. D, E_g and $S_{Par.}$ of prepared films.

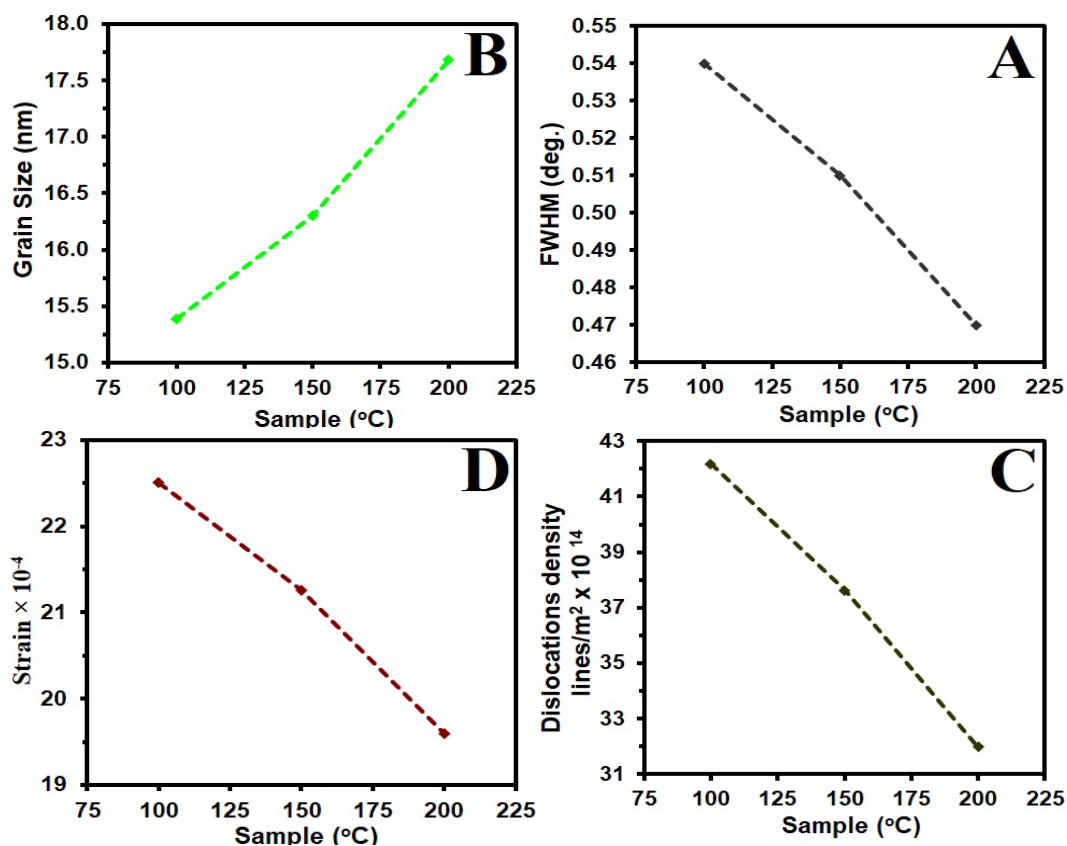| Specimen °C	2 θ (°)	(hkl) Plane	FWHM (°)	E_g (eV)	*D*(nm)	δ (× 10^{14}) (lines/m^2)	ε (× 10^{-4})
100	34.18	100	0.54	1.59	15.39	42.18	22.51
150	34.17	100	0.51	1.51	16.30	37.62	21.26
200	34.12	100	0.47	1.44	17.68	31.99	19.60

Fig. 3. FWHM (a) D (b) δ (c) ε (d) of the grown films.

AgO thin films with surface morphological qualities after being annealed at (100, 150, and 200) °C Scanner probe microscopy was used to perform the surface morphological analysis. The AFM pictures are shown in Fig. (4) (A_1, A_2, and A_3). Spectrophotometer and atomic force microscopy. Due to annealing at 200°C, the average particle size P_{av} behaved similarly and reduced from 76.9 nm to 46.5 nm. Due to annealing at 200°C, the surface roughness R_a exhibited the same behavior and dropped from 8.77 nm to 4.46 nm. With annealed 200°C, RMS roughness decreased from 7.33 nm to 3.64 nm. Figure 3 provides AFM parameters P_{AFM} for AgO thin films annealing at (100, 150, and 200) °C. Table 2 lists the AFM values.

Table 2. P_{AFM} of deposit films.

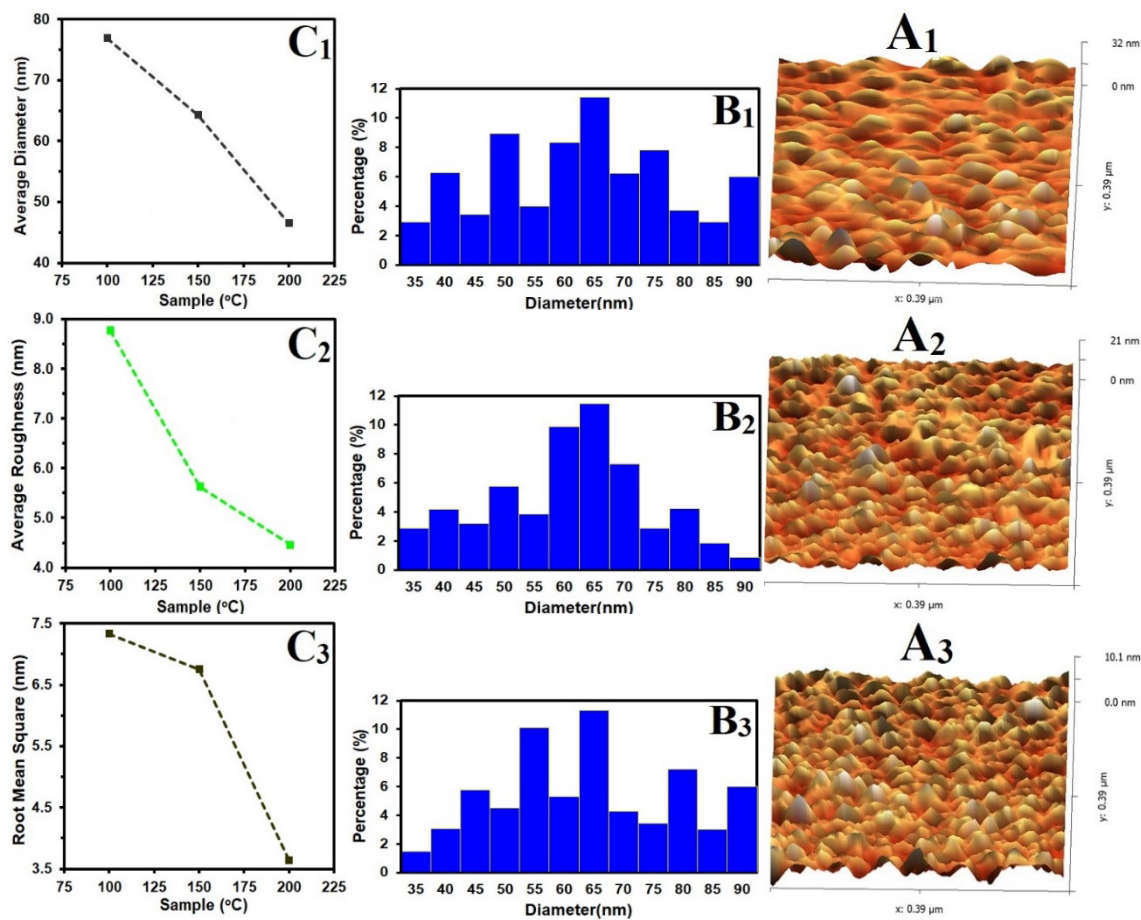| Specimen °C	P_{av} nm	R_a (nm)	RMS (nm)
100	7.9	8.77	7.33
150	64.3	5.63	6.75
200	46.5	4.46	3.64

Fig. 4. AFM surface morphological analysis of AgO

AgO's cluster structure is depicted in the SEM picture of AgO Figure 5. It is seen that as T_{an} increases, the size of clusters increases.
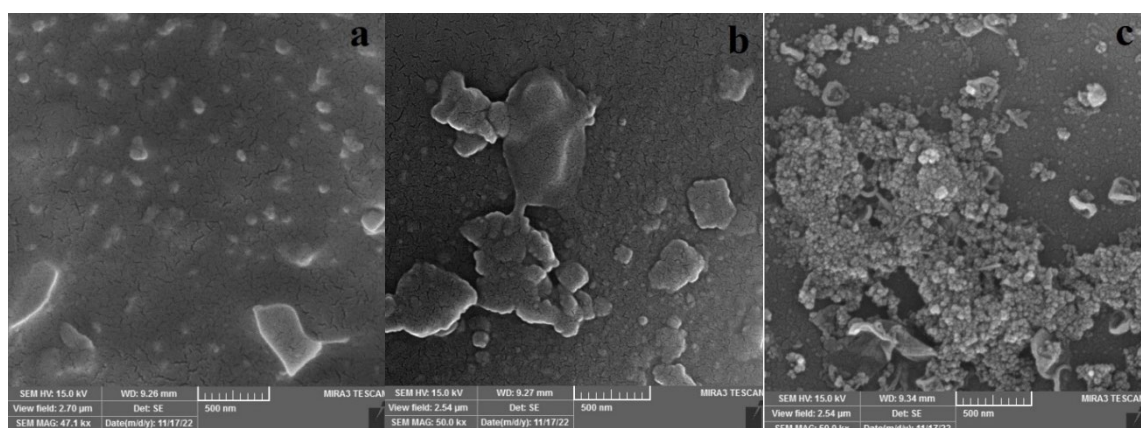

Fig. 5. SEM images of AgO: a 100 °C, b 150 °C nm, c 200 °C.

Film transmittance demonstrates Excellent optical transparency with values of 73 and 69% in the visible area for films annealed at 200 °C and 100 °C, respectively [12]. The relationship between the film's measured absorbance (A) and transmittance (T) is [36-38]:

$$A = \log\left(\frac{1}{T}\right) = \left(\frac{I}{I_o}\right) \tag{4}$$

where (I) is the transmitted light and (I_o) is the incident light. The dependency of the optical absorbance on wavelength is depicted in Figure (5). films with higher absorption in the UV region (shorter wavelength side) and lower absorption (visible area) [37].Tthe rise in annealing temperature increases absorbance. Figure (6) displays the transmittance spectrum of the intended films. It was discovered that the transmittance fell off as the annealing temperature rose [13].
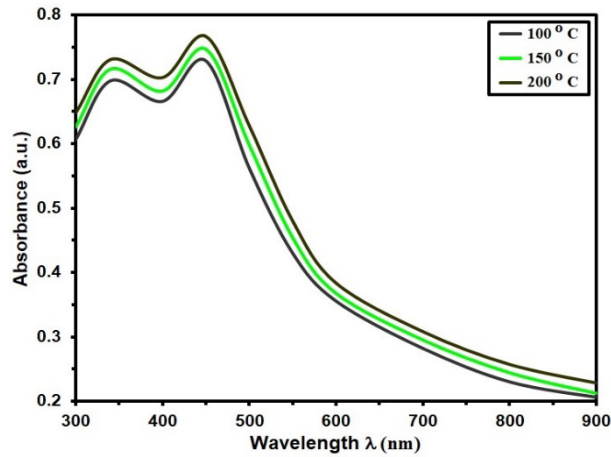
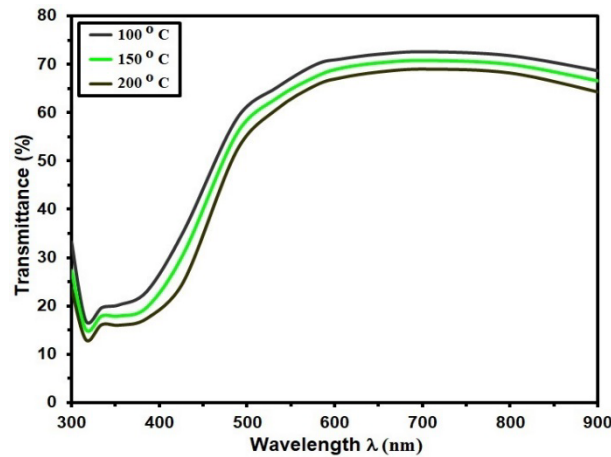Fig. 6. Absorbance of grown films.

Fig. 7. Transmittance of grown films.

The absorption coefficient (α) were specified by equation [39-41].

$$\alpha = (2.303 \times A)/t \tag{5}$$

where (t) is the thickness of the film, A is a constant. Plotting (α) against wavelength (λ) in Figure (8) indicates that for all films in the visible region, $\alpha > 4 \times 10^4$ cm^{-1}. This indicates that the transition must be direct electronic [40, 41]. Since this state's characteristics are what cause electrical conduction, to be significant. Furthermore, figure 6 demonstrates that the annealed 200°C films have a higher value of (α) than the 100°C annealed films. A decrease in the number of flaws and an increase in D could cause the absorbance to decrease with an increase in annealing degree [11].

The relationship that was utilised to compute the optical energy gap(E_g) of AgO is [42-43]:

$$(\alpha h\nu) = A\left(h\nu - E_g\right)^{\frac{1}{2}} \tag{6}$$

where $h\nu$ is the photon energy, A is a constant, the relations are plotted between $(\alpha h\nu)^2$ and photon energy ($h\nu$), E_g decreases as T_{an} increases. The obtained values of Eg (1.59, 1.51 and 1.044) eV agree with those reported for AgO thin films prepared by other techniques [11].
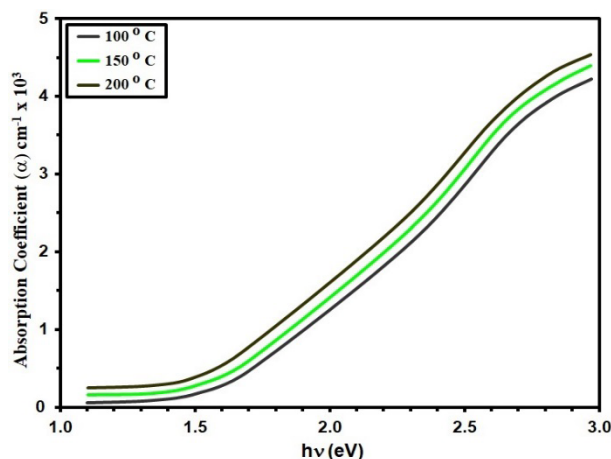
Fig. 8. α of the prepared films.
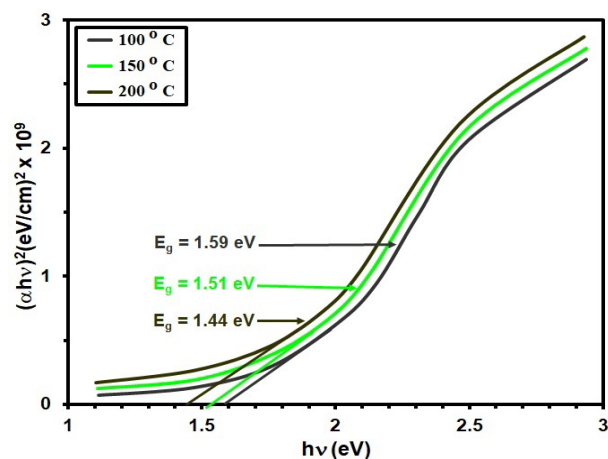
Fig. 9. (αhν)2 versus hν of grown films.

Extinction coefficient (K) was calculated using the related [45, -46].

$$k = \frac{\alpha\lambda}{4\pi} \tag{7}$$

Figure 10 displays K values. It has been noted that the spectrum shape of K and (α) are identical. T_{an} affected the K value at the visible region. For example, the value of K at 450 nm at 100°C is (0.564), whereas for 150°C at the same wavelength is (0.0.544), and at 200°C, is (0. 526). The extinction coefficient decreases as annealing temperature increases for the film [47].

The refractive index (n) measures how fast light travels in a vacuum compared to how fast it travels through materials that do not absorb light. The equation was used to get the value of n. [48, 49]:

$$n = (\frac{1+R}{1-R}) + \sqrt{\frac{4R}{(1-R)^2} - k^2} \tag{8}$$

Figure 11 acquired the value of n in the visible region dependent on the film treatment technique. The value of (n) at (450) nm at (100°C) is (2.907) while at 150°C at the same wavelength is (2.825) and at (200°C) is (2.774).

It is clear that n decreases with T_{an} increased [50].
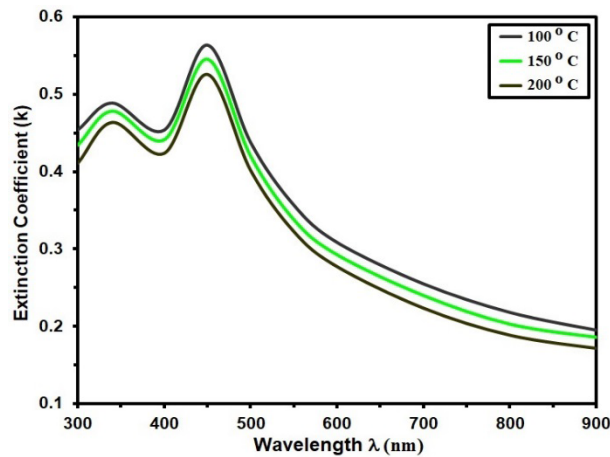
Fig. 10. k of the deposit films.
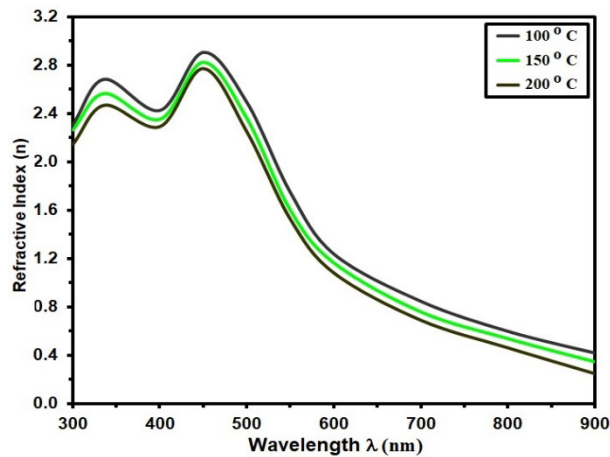
Fig. 11. n of the grown films.

Figure (12) offers the relationship between resistance via time of AgO annealed at (100, 150 and 200) °C at 300 ppm and at operating temperature of 120 °C. An oxidation process results from hydrogen (H_2) molecules deposited on the surface. The release of bonded electrons to the surface by certain O^{2+} ions will cause the electrons to start drifting back to the conduction band [52], increasing resistance and improving the potential wall under these circumstances [51]. Additionally, it was observed that the film AgO that has been annealed at 200 °C has the largest R, which is directly related to the film sensitivity and the strongest resistance to the gas flow [52, 53].

$$Sensitivity = \frac{\Delta R}{R_g} = \left| \frac{R_g - R_a}{R_g} \right| \times 100 \text{ %} \tag{9}$$

Fig. 12. Dynamic Resistance Change of AgO film annealed at (100, 150 and 200) °C.

The sensitivity plots as function varying annealed at (100, 150 and 200) °C is shown in figure (13) after exposure to Hydrogen gas. Due to the recomb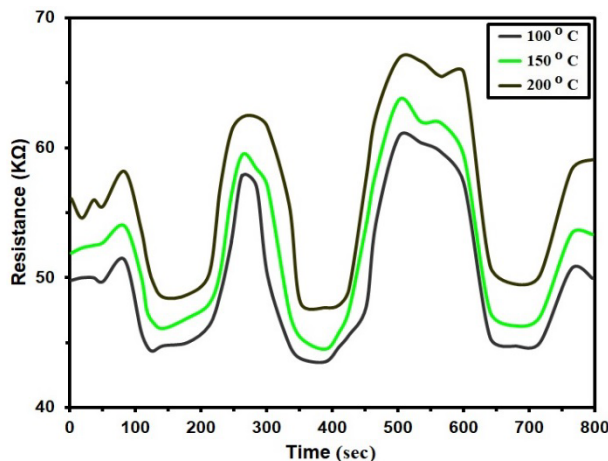ination process between the charge carriers of holes and electrons released from oxygen, it is discovered that the sensitivity reduces with increasing annealing temperature in relation to the rising electrical resistance of the film [54]. For different annealed at (100, 150, and 200) °C, respectively, the sensitivity dropped from 36.8% to 15.6% for 300 ppm, from 30.1% to 13.1% for 200 ppm, and from 23.5% to 3.8% for 100 ppm [55].
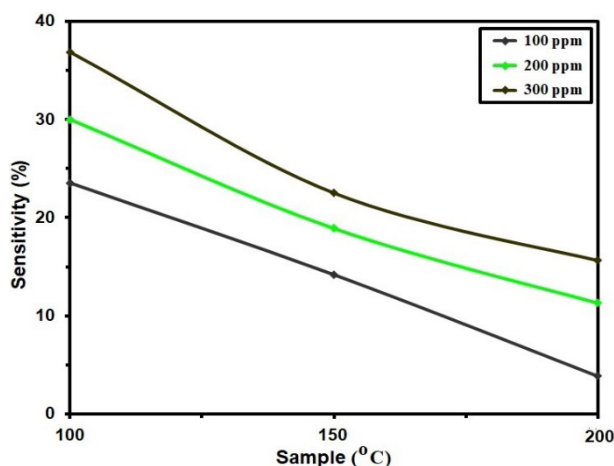
Fig. 13. Sensitivity of AgO annealed at (100, 150 and 200) °C.

4. Conclusion

AgO thin films were created using the thermal evaporation method. The (100) plane's XRD intensity increased as annealing temperature increased. While the strain rose from 22.50 to 19.60, the grain size for annealing at 100°C and 200°C is approximately (15.39–17.39) nm. AFM studies revealed a smooth R_a with RMS values decreasing from 7.33 nm to 3.64 nm from the film

annealed at 100°C and 200°C. Due to annealing at 200°C, the average particle size behaved similarly and reduced from 76.9 nm to 46.5 nm. According to optical spectroscopy results, annealed metal at 200°C had the highest absorption levels. Excellent optical transparency is demonstrated by the optical transmittance of the films, which have optical transmittance in the visible area of 73 and 69% for films annealed at 200 °C and 100 °C, respectively. Additionally, it was discovered that E_g reduced as T_{an} rose while the absorption coefficient increased. With a rise in film annealing temperature, extinction coefficient and refractive index drop. The best sensitivity was obtained for is annealed at 250 °C AgO was (36.8%) at an operating temperature of (120 °C) for 300 ppm gas concentration.

Acknowledgments

References

[1] K. Sivalingam, P. Shankar, G.K. Mani and J.B.B. Rayappan; Mater. Lett., 134, 47 (2014); https://doi.org/10.1016/j.matlet.2014.07.019

[2] A.R. Bushroa, R.G. Rahbar, H.H. Masjuki and M.R. Muhamad, Vacuum, 86, 1107 (2012); https://doi.org/10.1016/j.vacuum.2011.10.011

[3] N. R. C. Raju, K. J. Kumar and A. Subrahmanyam, J. Phys. D: Appl. Phys. 42, 135411 (2009); https://doi.org/10.1088/0022-3727/42/13/135411

[4] J. Tominaga, D. Buchel, C. Mihalcea, T. Shime,T. Fukaya, *MRS Proceedings*, 728, 7-3 (); https://doi.org/10.1016/j.tsf.2017.04.019

[5] K. H. Jebur, N. J. Mohammed, Al-Mustansiriyah Journal of Science, 32(4), 60-66 (2021); http://doi.org/10.23851/mjs.v32i4.993

[6] N. N. Jandow, N. F. Habubi, S. S. chiad, I. A. Al-Baidhany and M. A. Qaeed, International Journal of Nanoelectronics and Materials, 12 (1), 1-10 2019.

[7] N. N. Jandow, M. S. Othman, N. F.Habubi, S. S. Chiad, K. A. Mishjil, I. A. Al-Baidhany, Materials Research Express, 6 (11), (2020); https://doi.org/10.1088/2053-1591/ab4af8

[8] S. A. Hasan, J. A. Salman, S. S. Al-Jubori, Al-Mustansiriyah Journal of Science, 32(4), 21-25 (2021); http://doi.org/10.23851/mjs.v32i4.1034

[9] M. Fujimaki, K. Awazu and J. Tominaga; J. Appl. Phys., 100, 074303 (2006); https://doi.org/10.1063/1.2354329

[10] A. A. Z. Alaabedin, B. H. Hamza, A. Mu. Abdual-Majeed, S. F. Bamsaoud, Al-Mustansiriyah Journal of Science, 34 (3), 115-123 (2023); https://doi.org/10.23851/mjs.v34i3.1339

[11] F. Fang, Q. Li and J. K. Shang; Surface & Coatings Technology, 205, 2919 (2011); https://doi.org/10.1016/j.surfcoat.2010.10.068

[12] M. N. V. Ramesh, Y. Sundarayya, C. S. Sunandana, *Modern Physics Letters B*, 21 (28), 1933–1944 (2007); https://doi.org/10.1142/S0217984907014358

[13] J. F. Dierson and C. Rousselot, *Surface and Coatings Technology*, 200, 1–4, 276–279 (2005); https://doi.org/10.1016/j.surfcoat.2005.02.005

[14] Y. C. Her, Y. C. Lan, W. C. Hsu, S. Y. Tsai, *Journal of Applied Physics*, 96 (3), 1283–1288, (2004); https://doi.org/10.1063/1.1767978

[15] S. B. Rivers, G. Bernhardt, M. W. Wright, D. J. Frankel, M. M. Steeves, R. J. Lad, *Thin Solid Films*, 515 (24). 8684–8688 (2007); https://doi.org/10.1016/j.tsf.2007.03.139

[16] A. A. Schmidt, J. Offermann, R. Anton, *Thin Solid Films*, 281-282, 105–107 (1996); https://doi.org/10.1016/0040-6090(96)08586-0

[17] W. Wei, X. Mao, L. A. Ortiz, D. R. Sadoway, *Journal of Materials Chemistry*, 21 (2), 432–438 (2011); https://doi.org/10.1039/C0JM02214D

[18] N. R. C. Raju and K. J. Kumar, *Journal of Raman Spectroscopy*, 42 (7), 1505–1509 (2011); https://doi.org/10.1002/jrs.2895

[19] Y. Chiu, U. Rambaby, M. H. Hsu, H. P. D. Shieh, C. Y. Chen, H. H. Lin, *Journal of Applied hysics*, 94 (3), 6 (2003); https://doi.org/10.1063/1.1589178

[20] A. J. Varkey , A. F. Fort, *Solar Energy Materials and Solar Cells*, 29 (3), 253–259 (1993); https://doi.org/10.1016/0927-0248(93)90040-A

[21] X. Y. Gao, S. Y.Wang, J. Li et al., *Thin Solid Films*, 455, 438–442 (2004); https://doi.org/10.1016/j.tsf.2003.11.242

[22] Mohammed Ahmed Mohammed, Wasna'a M. Abdulridha, Ahmed N. Abd, *Journal of Global Pharma Technology*, 10 (03), 613-619, (2018); https://doi.org/10.1016/j.mssp.2018.106167

[23 T. Kikukawa, A. Tachibana, H. Fuji, J. Taminaga, Jpn. J. Appl. Phys., Part 1, 42, 1038 (2003); https://doi.org/10.1143/JJAP.42.1038

[24] F. A. Jasima , Z. S. A. Mosa, N. F. Habubi, Y. H. Kadhim, S. S. Chiad, Digest Journal of Nanomaterials and Biostructures, 18 (3), 1039–1049 (2023); https://doi.org/10.15251/DJNB.2023.183.1039

[25] N. Yamamoto, S. Tonomura, T. Matsuoka, H. Tsu- bomura, Japanese Jour- nal of Applied Physics, 20 (4), 721-726 (1981); http://dx.doi.org/10.1143/JJAP.20.721

[26] S. S. Chiad, N. F. Habubi, W. H. Abass, M.H. Abdul-Allah, Journal of Optoelectronics and Advanced Materials, 18(9-10), 822-826, (2016).

[27] E. S. Hassan, K. Y. Qader, E. H. Hadi, S. S. Chiad, N. F. Habubi, K. H. Abass, Nano Biomedicine and Engineering, 12(3), pp. 205-213 (2020); https://doi.org/10.5101/nbe.v12i3.p205-213

[28] M. D. Sakhil, Z. M. Shaban, K. S. Sharba, N. F. Habub, K. H. Abass, S. S. Chiad, A. S. Alkelaby, NeuroQuantology, 18 (5), 56-61 (2020); https://doi.org/10.14704/nq.2020.18.5.NQ20168

[29] Y. Ida, S. Watase, T. Shinagawa, M. Watanabe, M. Chi- gane, M. Inaba, A. Tasaka,
 M. Izaki, Chemistry of Materials, 20 (4) 1254-1256 (2008); http://dx.doi.org/10.1021/cm702865r

[30] N. Y. Ahmed, B. A. Bader, M. Y. Slewa, N. F. Habubi, S. S. Chiad, NeuroQuantology, 18(6), 55-60 (2020); https://doi.org/10.1016/j.jlumin.2021.118221

[31] Khadayeir, A. A., Hassan, E. S., Mubarak, T. H., Chiad, S.S., Habubi, N. F., Dawood, M.O., Al-Baidhany, I. A., Journal of Physics: Conference Series, 1294 (2) 022009(2019); https://doi.1088/1742-6596/1294/2/022009

[32] A. J. Ghazai, O. M. Abdulmunem, K. Y. Qader, S. S. Chiad, N. F. Habubi, AIP Conference Proceedings 2213 (1), 020101 (2020); https://doi.org/10.1063/5.0000158

[33] H. A. Hussin, R. S. Al-Hasnawy, R. I. Jasim, N. F. Habubi, S. S. Chiad, Journal of Green Engineering, 10(9), 7018-7028 (2020); https://doi.org/10.1088/1742-6596/1999/1/012063

[34] S. S. Chiad, H. A. Noor, O. M. Abdulmunem, N. F. Habubi, M. Jadan, J. S. Addasi, Journal of Ovonic Research, 16 (1), 35-40 (2020). https://doi.org/10.15251/JOR.2020.161.35

[35] H. T. Salloom, E. H. Hadi, N. F. Habubi, S. S. Chiad, M. Jadan, J. S. Addasi, Digest Journal of Nanomaterials and Biostructures, 15 (4), 189-1195 (2020); https://doi.org/10.15251/DJNB.2020.154.1189

[36] R. S Ali, N. A. H. Al Aaraji, E. H. Hadi, N. F. Habubi, S. S. Chiad, Journal of Nanostructuresthis link is disabled, 10(4), 810–816 (2020); https://doi: 10.22052/jns.2020.04.014

[37] A. A. Khadayeir, R. I. Jasim, S. H. Jumaah, N. F, Habubi, S. S. Chiad, Journal of Physics: Conference Series,1664 (1) (2020); https://doi.org/10.1088/1742-6596/1664/1/012009

[38] S. S Chiad,, A. S. Alkelaby, K. S. Sharba,, Journal of Global Pharma Technology, 11 (7), 662-665, (2020); https://doi.org/10.1021/acscatal.1c01666

[39] Chiad, S.S., Noor, H.A., Abdulmunem, O.M., Habubi, N.F., Journal of Physics: Conference Series 1362(1), 012115 (2019); https://doi.org/10.1088/1742-6596/1362/1/012115

[40] R. S. Ali, M. K. Mohammed, A. A. Khadayeir, Z. M. Abood, N. F. Habubi and S. S. Chiad, Journal of Physics: Conference Series, 1664 (1), 012016 (2020); https://doi:10.1088/1742-6596/1664/1/012016

[41] A. S. Al Rawas, M. Y. Slewa, B. A. Bader, N. F. Habubi, S. S. Chiad, Journal of Green Engineering,10 (9), 7141-7153 (2020); https://doi.org/10.1021/acsami.1c00304

524

[42] K. Y. Qader, R. . Ghazi, A. M. Jabbar, K. H. Abass, S. S. Chiad, Journal of Green Engineering, 10 (10), 7387-7398, 2020. https://doi.org/10.1016/j.jece.2020.104011

[43] R. S. Ali, H. S. Rasheed, N. F. Habubi, S.S. Chiad, Chalcogenide Letters, , 20 (1), 63–72 (2023; https://doi.org/10.15251/CL.2023.201.63

[42] A. Ghazai, K. Qader, N. F. Hbubi, S. S. Chiad, O. Abdulmunem, IOP Conference Series: Materials Science and Engineering, 870 (1), 012027 (2020); https://doi.org/ 10.1088/1757-899X/870/1/012027

[43] B. A. Bader, S. K. Muhammad, A. M. Jabbar, K. H. Abass, S. S. Chiad, N. F. Habubi, J. Nanostruct, 10(4): 744-750, (2020); https://doi.org/ 10.22052/JNS.2020.04.007

[44] O. M. Abdulmunem, A. M. Jabbar, S. K. Muhammad, M. O. Dawood, S. S. Chiad, N. F. Habubi, Journal of Physics: Conference Series,1660 (1), 012055 (2020); https://doi.org/ 10.1088/1742-6596/1660/1/012055

[45] E. H. Hadi, M. A. Abbsa, A. A. Khadayeir, Z. M. Abood, N. F. Habubi, and S.S. Chiad, Journal of Physics: Conference Series, 1664 (1), 012069 (2020); https://doi.org/ 10.1088/1742-6596/1664/1/012069

[46] M. S. Othman, K. A. Mishjil, H. G. Rashid, S. S. Chiad, N. F. Habubi, I. A. Al-Baidhany, Journal of Materials Science: Materials in Electronics, 31(11), 9037-9043 (2020); https://doi.org/10.1007/s10854-020-03437-0

[47] S. S. Chiad, T. H. Mubarak, International Journal of Nanoelectronics and Materials, 13 (2), 221-232 (2020).

[48] Hassan, E.S., Mubarak, T.H., Chiad, S.S., Habubi, N.F., Khadayeir, A.A., Dawood, M.O., Al-Baidhany, I. A. , Journal of Physics: Conference Series, 1294(2), 022008 (2019); https://doi.1088/1742-6596/1294/2/022008

[49] M.O. Dawood, S.S. Chiad, A.J. Ghazai, N.F. Habubi, O.M. Abdulmunem, AIP Conference Proceedings 2213, 020102,(2020); https://doi.org/10.1063/5.0000136

[50] S. Singh, A. Sharma, P. Kumar, R. Thangavel, Journal of Materials Science: Materials in Electronics, 29 (14), 11967-11974 (2018); https://doi.org/10.1007/s10854-018-9476-0.

[51] R. Bharti, V. Sharma, A. Kumar, P. Saini, " Materials Today: Proceedings, 5 (2) 5296-5301 (2018); https://doi.org/10.1016/j.matpr.2017.12.228.

[52] A. A. Khadayeir, E. S. Hassan, S. S. Chiad, N. F. Habubi, K. H. Abass, M. H. Rahid, T. H. Mubarak, M. O. Dawod, and I.A. Al-Baidhany, Journal of Physics: Conference Series 1234 (1), 012014, (2019); https://doi.1088/1742-6596/1234/1/012014

[53] N. Y. Ahmed, B. A. Bader, M. Y. Slewa, N. F. Habubi, S. S. Chiad, NeuroQuantology, 18(6), 55-60 (2020); https://doi.org/10.14704/nq.2020.18.6.NQ20183

[54] E. H. Hadi, D. A. Sabur, S. S. Chiad, N. F. Habubi, K., Abass, Journal of Green Engineering, 10 (10), 8390-8400 (2020); https://doi.org/10.1063/5.0095169

[55] H. Yin, et al., Journal of Materials Science: Materials in Electronics, 31(16) 14280-14288 (2020); http://dx.doi.org/10.1007/s10854-020-03734-5